Neutron Measurements with a
Shielded Source

and

Measured and Theoretical Errors for
Multiplicity Counting

Physics 492R Capstone Project Report

Matthew McArthur

Advisor: Dr. Lawrence Rees

November 3, 2014

Intoduction to Projects

As an undergraduate I have completed two major projects. I have written up papers to summarize each of them. The first project was completed as a member of the BYU nuclear physics group under the advisement of Dr. Lawrence Rees and Bart Czirr. The purpose of the project was to analyze the effects of neutron shielding in the form of polyethylene and borated polyethylene on the ability to detect fission sources, as well as to compare these results with the results of simulations using Monte Carlo Neutral Particle (MCNP) code. The second project was carried out under the advisement of Malte Gottsche, a PHd candidate at the Carl Friedrich von Weizsacker-Centre for Science and Peace Research at the University of Hamburg. The purpose of this project was to analyze diferent methods of calculating the uncertanties of neutron multiplicity counting simulations done using MCNP.

Neutron Shielding

The motivation for this project began when data was collected using a lithium-glass detector developed by the group for a fission source that was highly shielded with polyethylene. When the results of the experiment were compared with a simulation using MCNP we found that MCNP had overestimated the results by a factor of two. Due to the importance of MCNP calculations in a wide range of applications including calculations done to determine the ability that neutron detectors used for portal monitoring to stop the importation of Special Nuclear Materials (SNM) have to detect shielded sources, we decided it was important to fully analyze the effects of shielding on the efficiency of our detectors as well as to analyze the ability of MCNP to model highly shielded sources. The paper included details more of the motivation as well as the methods and results of the project.

Neutron Multiplicity Counting

This project was completed as part of a three month internship with the Carl Friedrich von Weizsacker-Centre for Science and Peace Research at the University of Hamburg working with a PHd candidate Malte Gottsche on nuclear warhead disarmament verification using an information barrier. Specifically I was working with him on using neutron multiplicity counting to determine the fissile mass of plutonium or uranium, which could be used in conjunction with other techniques to authenticate a nuclear warhead in a non-intrusive way gleaning little or no information on the construction of nuclear weapons by the authentication party. The motivation for this authentication comes from the desire of many nations, and as stipulated in the Nonproliferation Treaty, to move toward nuclear disamament. However, in the current disarmament process nuclear warheads are verified inderectly via their delivery vehicles. A non-intrusive authentication could therefore be used in disarmament by authenticating both

the pre and post-dismantled weapon. The largest nuclear weapons states by far are the United States and Russia, yet they are slow to move toward disarmament. Part of this reluctance is due to the low level of trust in eachother when it comes to disarmament. Using this verification technique a third party would be able to verify the actual disarmament of nuclear weapons without gaining any state secrets and allowing there to be more confidence and trust between the United States and Russia with regard to nuclear disarmament.

Important to this verification process is the application of neutron multiplicity counting to determine the fissile mass of the plutonium or uranium being used in the nuclear weapon. MCNP is often used to simulate neutron multiplicity counting experiments. As part of my internship I wrote programs to analyze both the experimental and simulated data collected and determine the singles, doubles and triples rates and their associated uncertanties. However, their were several existing methods to determine the uncertanties for the simulated data, so as part of my project I analyzed the diferent methods and compared the results with the calculated uncertanties. The techniques analyzed and their results are included in the attached paper.

Neutron Measurements with a Shielded Source

November 3, 2014

Abstract

Using the combination of a neutron sensitive ^{6}Li glass scintillator detector with a neutron insensitive ^{7}Li glass scintillator detector we are able to accurately measure the neutron capture rate of our ^{6}Li detector. We used this detector with a Cf neutron source to measure the effects that both polyethylene and 5% borated polyethylene shielding has on our capture rates. Both of these measurements were compared with MCNP calculations to determine how well the calculations simulated the measurements, particularly when the source is highly shielded. MCNP is shown to have a general tendency to underestimate detector efficiency with polyethylene shielding. For pure polyethylene it underestimates the measured value at an average of 10%. This increases to an average of 18% for borated polyethylene.

1 Introduction and Motivation

Currently radiation portal monitoring (RPM) systems are used to help prevent the importation of Special Nuclear Materials (SNM). Neutron detectors are used as part of these systems to interdict the importation of materials, such as plutonium, that have high spontaneous fission rates. Rees and Czirr [Rees] stressed the importance of these detectors to be able to be sensitive not only to bare fission sources, but also to shielded sources. Shielded sources are especially important as any illegally imported material will likely be shielded to avoid detection. Polyethylene is a well known neutron moderator and used in many shielding applications because of its high hydrogen content. High hydrogen content is desirable because hydrogen-neutron collisions cause the neutron to lose half of its energy on average per collision. To improve the absorption of neutrons in the polyethylene, boron can be added, which has a high neutron capture cross section. This has been found to be a much better shielding material [poly-boron]. We constructed a moderated lithium-glass detector that is sensitvie to both high and low energy fission neutrons. Using this detector, we measured teh effects of shielding a ^{252}Cf fission source with both polyethylene and borated polyethylene. We compare the experimental results with simulations using Monte Carlo Neutral Particle (MCNP) code [MCNP].
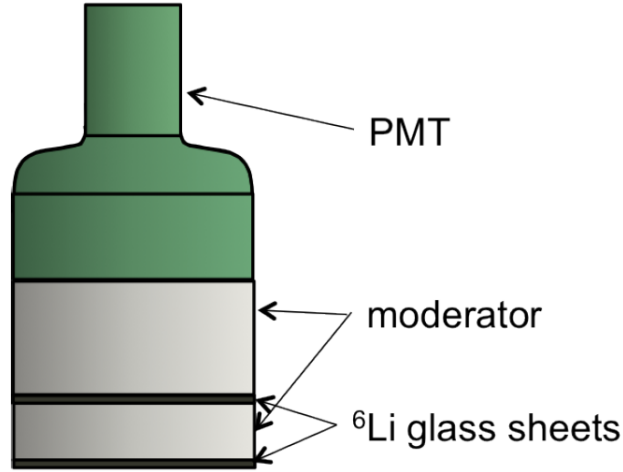
Figure 1: Detector geometry

2 Experimental Methods

2.1 Detectors

Two neutron detectors were used in conjunction with each other for our data collection. The first consists of two pieces of ^{6}Li-doped glass scintillator each 1 mm thick and 5 inches in diameter each. The first piece of glass is placed on the front end of the detector followed by 1 inch of lucite moderator. The second sheet of glass scintillator is placed on top of the lucite and then 3 more inches of lucite moderator is added. The glass and lucite all have a 5 inch diameter. Finally, on top of the lucite moderator is placed a 5-inch Adit photomultiplier tube as shown in Fig. 1. The ^{6}Li in the glass scintillator has a large capture cross section for lower-energy neutrons. The neutron capture and subsequent fission process is as follows:

$$n +^6 Li \rightarrow \alpha(2.056 \text{MeV}) +^3 H(2.729 \text{MeV}) \tag{2.1}$$
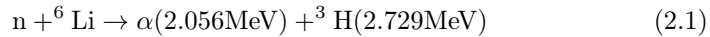
The alpha particle has a range of 7 μm in the lithium glass and the triton has a range of 40 μm, therefore both particles will generally deposit all of their energy in the 1 mm thick piece of glass. The energy from these charged particles will cause scintillation that creates a large, wide peak in the photomultiplier tube. If this pulse rises above a set threshold, the pulse will be recorded as by a signal digitizer. Two sheets of glass are used because the neutrons can vary greatly in energy. The lucite moderator is high in hydrogen. As neutrons collide with the hydrogen, they will change both energy and direction. The design of the detector allows for high energy neutrons that will likely pass through the first piece of glass to be slowed down and either backscatter into the first piece

2
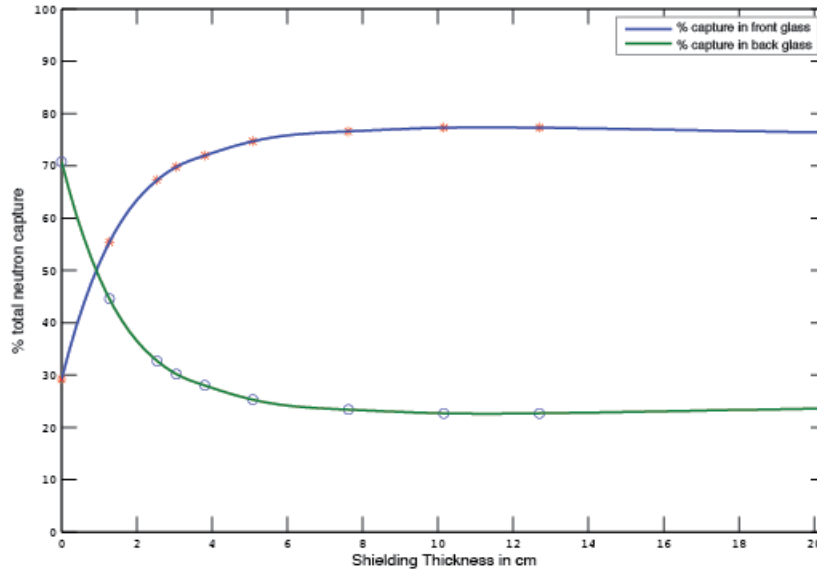
Figure 2: MCNP calculation of percentage of lithium capture taking place in each sheet of glass as a function of shielding thickness.

of glass or capture in the second piece. Low energy neutrons will mostly be absorbed by the first piece of glass. This can be seen in Fig. 2 which depicts an MCNP calculation of the fraction of neutron captures in lithium that take place in each sheet of glass. Over 70% of the higher energy unshielded neutrons are captured in the second piece, however, as shielding increases and the energy of neutrons leaving the shielding decreases, nearly all of the neutron capture occurrs in the first sheet. This allows for high sensitivity over a broader range of neutron energies.

2.1.1 Gamma Discrimination

For our application, this detector must also be able to differentiate between neutrons and gamma rays. Gamma rays can Compton scatter in the glass and transfer energy to electrons which can excite the scnitillator and create a light pulse. Because the range of electrons of this energy is about 1 mm in the glass, it is not likely that all of their energy will be deposited within the glass itself. However, when it does occur, these pulses will cause an event to be recorded just as a neutron would. Neutron pulses and gamma pulses can be distinguished in the data analysis by comparing the shapes of the pulses. Pulses caused by neutrons are wider and have a longer tail where pulses caused by gammas are much narrower. This allows for the process of pulse-shape discrimination to be applied to discriminate between neutrons and gammas.[wallace]

To further reduce gamma events, a second detector was built with exactly the

same dimensions as the first detector, but replacing the ^{6}Li glass scintillator with ^{7}Li glass scintillator. The ^{7}Li glass scintillator has the same gamma sensitivity, but it lacks the high neutron capture cross section making it insensitive to neutrons. This is then used in conjunction with the first detector to allow the subtraction of source-related gamma events.

The two detectors were first gain matched by adjusting the photomultiplier tube voltages and using a ^{60}Co source. Every set of shielding data for a given configuration consisted of four runs of data collection. Two background runs were taken, first using the ^{6}Li detector and then the ^{7}Li detector. Two runs with the ^{252}Cf fission source were also taken, again with the ^{6}Li then the ^{7}Li detector. The total number of source neutrons detected, T, was then calculated as follows:

$$\left[^6\text{Li(Cf)-}^7\text{Li(Cf)}\right] - \left[^6\text{Li(Bkg)-}^7\text{Li(Bkg)}\right] = \text{T} \tag{2.2}$$

In other words, the total number of source neutrons detected equals the total number of neutrons captured in the ^{6}Li detector minus the total number of background neutrons. The two-detector design creates a high level of confidence in our measurement of the total number of source neutrons T, which allows us to calculate the efficiency of the detector.

2.2   Experimental Setup

Another difficulty with making accurate neutron measurements is that of "room return" caused by walls, floors, etc., that readily reflect neutrons and cause overestimates of detector efficiency. To minimize this effect, we placed our detector, shielding, and source on top of a 20 ft scissor lift. This separated our experiment from all walls and floors and concrete objects which are the major neutron-reflecting materials.

On the scissor lift the detector was placed facing downward on a thin steel sheet 4 ft above the floor of the lift. The source was elevated 48 cm above the floor, 55 cm below the detector. 12×12×1 inch slabs of borated polyethylene and 12×12×1.18 inch slabs of pure polyethylene were used as shielding. The source was placed in a small slot in the center of two slabs of shielding. Data were taken with the bare source and with two, four, six, eight, ten, twelve, and sixteen slabs of shielding equally divided above and below the source.

MCNP was used to model each of these configurations. The exact chemical makeup of the borated polyethylene was measured using x-ray photoelectron spectroscopy and verified by the distributor. By weight percentage the borated polyethylene used was 11.60% hydrogen, 62.20% carbon, 22.00% oxygen and 5% boron.

3   Results/Data

3.1   Pure Polyethylene

We describe our results in terms of "practical intrinsic efficiency," defined as the ratio of detected neutrons to neutrons emitted from the source into the solid angle subtended by the detector. The detector has a maximum measured practical intrinsic efficiency of 53.51% with 3 cm of polyethylene shielding above the source. The decrease in the neutron detection rate with larger amounts of shielding occurs solely because of the large number of neutrons that are absorbed in the shielding. The lowest practical intrinsic efficiency occurs with 24 cm of shielding which is the last measured data point. At this level of shielding, the practical intrinsic efficiency was measured to be 1.45%. Although the efficiency has dropped off considerably the neutron counting rate is over 100 times the measured neutron background rate.

The MCNP simulations showed a general tendency to underestimate the measured efficiency, as seen in Fig. 3. The bare source comparison showed an underestimation of 15%. With only one slab of shielding this underestimation dropped to 4% and then gradually increased with every layer of shielding until it reached 29% at 24 cm.
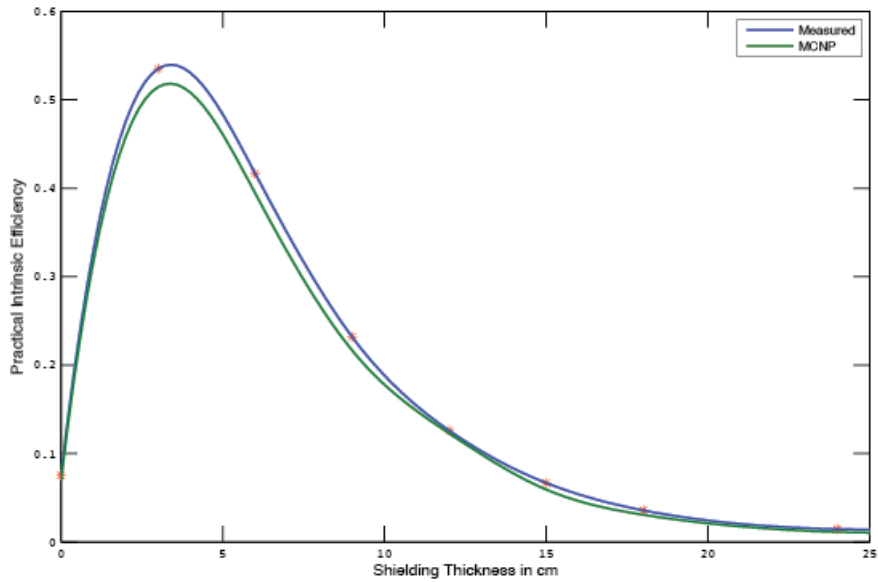
Figure 3: MCNP vs. measured practical intrinsic efficiency for polyethylene.

3.2 Borated Polyethylene

The neutron detection rate was about a factor of two less than that of pure polyethylene for the same configuration. The detector's practical intrinsic efficiency was at a maximum at 27% with 2.54 cm of shielding. It then followed a similar curve to pure polyethylene ending at 1.37%. This means that it is detecting neutrons at a rate about 80 times that of our measured neutron background rate.

Once again MCNP showed a tendency to underestimate the measured efficiency.
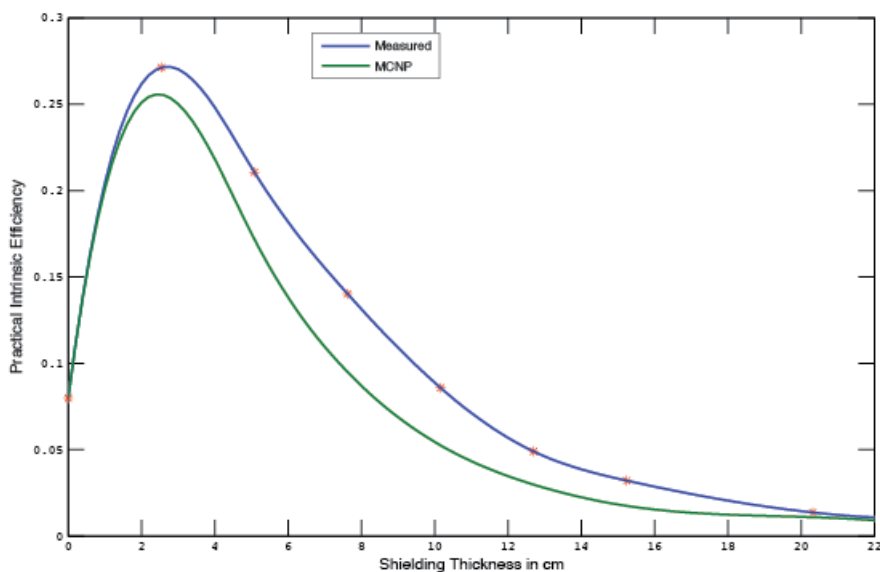
Figure 4: MCNP vs. measured practical intrinsic efficiency for borated polyethylene.

At 2.54 cm of shielding MCNP underestimates the measured efficiency by 5.5%. This number rapidly increases to around 20% for 7.62-15.24 cm of shielding with a high of 28% at 15.24 cm. At 20.32 cm of shielding the MCNPcalculated efficiency rises above the measured value overestimating the efficiency by 17%.

Also, MCNP calculations were done to compare the response of a typical ^{3}He detector to the one used in this experiment. The detector-source distance was chosen so that the solid angle of the ^{3}He tube was that of one of our typical experimental runs. The calculation showed that the ^{6}Li glass detector has a much higher efficiency with all levels of shielding. The ^{3}He tube reached its peak practical intrinsic efficiency of 9.14% with one slab of shielding as shown in Fig. 5.
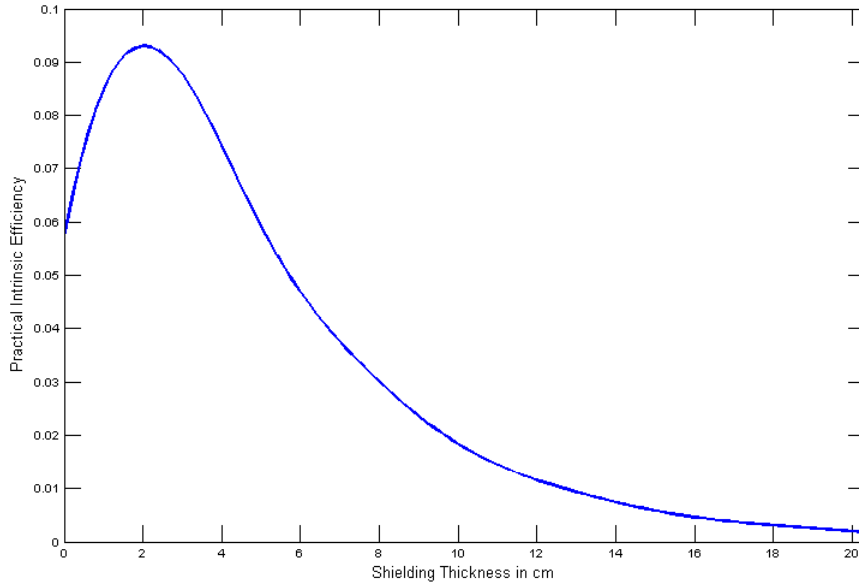
Figure 5: MCNP calculation of a ^{3}He tube with borated polyethylene shielding.

4 Conclusion

Both pure polyethylene and borated polyethylene give an initial increase in neutron detection efficiency as many neutrons are thermalized, but a large amount are still able to escape the shielding without being captured. As shielding is added, the detector's practical intrinsic efficiency quickly decreases as more and more neutrons are captured and never escape the shielding.

This detector is capable of detecting neutron fission sources comparable to ^{252}Cf witth at least 24 cm of pure polyethylene of 20.3 cm of borated polyethylene with counting rates well over the neutron background rate.

MCNP does a good job at modeling polyethylene and borated polyethylene with a general tendency of underestimating detector efficiency. For pure polyethylene it underestimates the measured value at an average of 10%. This increases to an average of 18% for borated polyethylene.

Borated polyethylene makes a better neutron shield with an increase in neutron absorption by a factor of 2 on average.

References

[1]

[Rees]   Lawrence B. Rees and J. Bart Czirr, Optimizing moderation of
              He-3 neutron detectors for shielded fission sources, *Nuclear In-
              struments & Methods in Physics Research A*, 691:72–80 (2012).

[poly-boron] Nolan Hertel, Courtney Harrison, Eric Burgett and Eric Grulke,
              Polyethylene-boron composites for radiation shielding applica-
              tions, *AIP Conference Proceedings*, 969:484–491 (2008).

[MCNP]   MCNP X-5 Monte Carlo Team. *MCNP-a general purpose Monte
              Carlo Nparticle transport code.* Los Alamos National Laboratory,
              LA-UR-03-1987, version 5 edition. April 2003 (the MCNP code can
              be obtained from the Radiation Safety Information Computational
              Center (RSICC), Oak Ridge, TN).

[wallace]   Adam Wallace. Lithium-glass neutron detection, April 2011,
              https://www.physics.byu.edu/docs/thesis/311.

Measured and Theoretical Errors for Multiplicity Counting

M. McArthur

December 7, 2014

Abstract

The method for arriving at the statistical errors for the mass, multiplication and alpha-n rate for a Pu source from a multiplicity counting measurement is explained. Next, three methods for calculating the errors from a simulation using MCNP-Polimi are presented and compared with the measured results. The three approaches considered here are: a multinomial distribution, a Poisson distribution, and a semi-empircal approach.

Introduction

Multiplicity counting is a technique used to determine the mass, the multiplication and the alpha-n rate which can be used to determine the actual weight of effective Pu-240 mass in a sample. This can be used as part of a nuclear warhead verification procedure. An important requirement is a knowledge of the uncertainty of the assayed effective Pu-240 mass. The uncertainty can be determined, but because the singles, doubles and triples rates used to calculate the mass, multiplication and alpha-n rate are inherently correlated, simple Gaussian error propogation might not suffice, and determinig the correct uncertanties becomes a challenge. Different approaches will be discussed here. The techniques and methods used are based on a paper by Dytlewski. [1]

Measured Errors

The covariance matrix for the singles, doubles and triples can be estimated directly in a measurement by taking collecting several data sets. The calculated singles, doubles and triples rates can then be compared to find the correlations between them through multiple runs. Mathematically the covariance matrix is

$$\text{Cov(SDT)} = \begin{bmatrix} \sigma_{S^2} & \sigma_{SD} & \sigma_{ST} \\ \sigma_{DS} & \sigma_{D^2} & \sigma_{DT} \\ \sigma_{TS} & \sigma_{TD} & \sigma_{T^2} \end{bmatrix}$$

1

where

$$\sigma_{SD} = \frac{1}{N-1}\left[\left(S_1 - \bar{S}\right)\left(D_1 - \bar{D}\right) + \left(S_2 - \bar{S}\right)\left(D_2 - \bar{D}\right) + ... + \left(S_N - \bar{S}\right)\left(D_N - \bar{D}\right)\right]$$
(1)

N is the number of data sets.

This represents the correlations between singles and doubles.

When performing these calculations one can see that there is a clear correlation between the singles, doubles and triples rates. An example covariance matrix that shows this coorelation is given in Table 1. The software that analyzes the measurement files performs the calculations this way and expresses the error as the Standard Error.

With the covariance matrix of singles, doubles and triples, the covariance matrix for the mass, multiplication and alpha is attained by using the matrix of the partial derivative of the same with respect to singles, doubles and triples.

$$\text{Cov}[\text{mM}\alpha] = A \cdot \text{Cov}[\text{SDT}] \cdot A^T \tag{2}$$

where

$$A = \begin{bmatrix} \frac{\partial m}{\partial S} & \frac{\partial m}{\partial D} & \frac{\partial m}{\partial T} \\ \frac{\partial M}{\partial S} & \frac{\partial M}{\partial D} & \frac{\partial M}{\partial T} \\ \frac{\partial \alpha}{\partial S} & \frac{\partial \alpha}{\partial D} & \frac{\partial \alpha}{\partial T} \end{bmatrix}$$

The diagonal of this matrix is then the variance of the mass, multiplication and alpha. The errors for mass, multiplication, and alpha are then expressed as the standard error in the measurement output file.

Theoretical Errors

Multiplicity counting experiments are often simulated using MCNP-Polimi which has the disadvantage of not performing mutiple cycles of data collection with the same conditions. Because of this it is impossible to find the covariance matrix by simply viewing the correlations through multiple runs. So a new technique is needed to find the covariance matrix theoretically.

In the analysis of the neutron pulse stream, the number of times that n counts are observed in each gate is recorded in a distribution. The signal-triggered gate, or the reals plus accidentals gate, distribution will be called P(n). The random triggered gate, or accidentals gate, distribution well be called Q(n). In the simulation only one P(n) and one Q(n) multiplicity distribution can be calculated. However, one can use the covariance matrix of these, which would need to be calculated through the application of a model as will be proposed later, to arrive at an estimated singles, doubles and triples covariance matrix. To find the covariance matrices of the singles, double and triples the three approaches considered are: a multinomial distribuition, a Poisson distribution, and a semi-empircal approach.

Multinomial Distribution

A multinomial distribution can be used to model the distribution if each gate that is opened is thought of as a trial. Each of these trials then has exactly one success for one of k categories, where the catagories are the possible multiplicities. This model assumes that the total number of counts is constant for every distribution.

Assuming a multinomial distribution, the covariance matrix of the P(n) distribution and Q(n) distribution can be found by:

$$\text{Cov(P(n))}_{ii} = p_i(1 - p_i) \sum_{n=0}^{max} P(n) \tag{3}$$

$$\text{Cov(P(n))}_{ij} = -p_i p_j \sum_{n=0}^{max} P(n) \tag{4}$$

where p_i is the probability of measuring multiplicity i given by:

$p_i = \frac{P(i)}{\sum P(n)}$

and

$$\text{Cov(Q(n))}_{ii} = p_i(1 - p_i) \sum_{n=0}^{max} Q(n) \tag{5}$$

$$\text{Cov(Q(n))}_{ij} = -p_i p_j \sum_{n=0}^{max} Q(n) \tag{6}$$

where here

$p_i = \frac{Q(i)}{\sum Q(n)}$

The Cov(P(n),Q(n)) and Cov(Q(n),P(n)) are taken to be independent and are set to zero in approximation. [1]

Two more matrices are necessary to find the covariance matrix for the singles, doubles and triples. The first we call X and is the matrix of partial derivatives of the singles, doubles and triples rates with respect to the reals plus accidentals distribution P(n), the second we call Y and is the matrix of partial derivatives of the singles, doubles and triples rates with respect to the accidentals distribution Q(n).

The equations used for singles, doubles and triples are the non deadtime corrected equations since in our simulation there was no deadtime simulated.

$$S = \frac{\sum_{n=0}^{max} P(n)}{t} \tag{7}$$

$$D = \frac{\sum_{n=0}^{max} nP(n) - \sum_{n=0}^{max} nQ(n)}{t} \tag{8}$$

3

$$T = \frac{\frac{\sum_{n=0}^{max} n(n-1)P(n)}{2} - \frac{\sum_{n=0}^{max} n(n-1)Q(n)}{2} - \sum_{n=0}^{max}(nQ(n))\left(\frac{\sum_{n=0}^{max} nP(n) - \sum_{n=0}^{max} nQ(n)}{\sum_{n=0}^{max} P(n)}\right)}{t}$$
(9)

The partial derivatives with respect to P(n) are:

$$\frac{\partial S}{\partial P(n)} = \frac{1}{t} \tag{10}$$

$$\frac{\partial D}{\partial P(n)} = \frac{n}{t} \tag{11}$$

$$\frac{\partial T}{\partial P(n)} = \frac{\frac{n(n-1)}{2} - \frac{\sum_{m=0}^{max} mQ(m)}{\sum_{m=0}^{max} P(m)}\left(n - \frac{\sum_{m=0}^{max} mP(m) - \sum_{m=0}^{max} mQ(m)}{\sum_{m=0}^{max} P(m)}\right)}{t} \tag{12}$$

And the partial derivatives with respect to Q(n) are:

$$\frac{\partial S}{\partial Q(n)} = 0 \tag{13}$$

$$\frac{\partial D}{\partial Q(n)} = -\frac{n}{t} \tag{14}$$

$$\frac{\partial T}{\partial Q(n)} = \frac{-\frac{n(n-1)}{2} + n\frac{\sum_{m=0}^{max} m(2Q(m)-P(m))}{\sum_{m=0}^{max} P(m)}}{t} \tag{15}$$

The X and Y matrices can then be constructed as follows using equations 10-15:

$$X = \begin{bmatrix} \frac{\partial S}{\partial P(1)} & \frac{\partial S}{\partial P(2)} & \cdots & \frac{\partial S}{\partial P(n)} \\ \frac{\partial D}{\partial P(1)} & \frac{\partial D}{\partial P(2)} & \cdots & \frac{\partial D}{\partial P(n)} \\ \frac{\partial T}{\partial P(1)} & \frac{\partial T}{\partial P(2)} & \cdots & \frac{\partial T}{\partial P(n)} \end{bmatrix}$$

$$Y = \begin{bmatrix} \frac{\partial S}{\partial Q(1)} & \frac{\partial S}{\partial Q(2)} & \cdots & \frac{\partial S}{\partial Q(n)} \\ \frac{\partial D}{\partial Q(1)} & \frac{\partial D}{\partial Q(2)} & \cdots & \frac{\partial D}{\partial Q(n)} \\ \frac{\partial T}{\partial Q(1)} & \frac{\partial T}{\partial Q(2)} & \cdots & \frac{\partial T}{\partial Q(n)} \end{bmatrix}$$

Then the covariance matrix of the singles, doubles and triples can be found using X and Y along with the covariance matrices of the distributions found in equations 3-6:

$$\text{Cov(SDT)} = X \cdot \text{Cov(P(n))} \cdot X^T + Y \cdot \text{Cov(Q(n))} \cdot Y^T \tag{16}$$

The equations for the variance of the singles, doubles and triples found by equation 16 are:

$$\sigma_S^2 = \sum_{n=0}^{max} \left[\frac{\partial S}{\partial P(n)} \sum_{m=0}^{max} \frac{\partial S}{\partial P(m)} \sigma_{mn} \right] = \frac{\left[\sum_{i=0}^{max} p_i(1-p_i) + \sum_{i=0}^{max} \sum_{j=0}^{max} -p_i p_j \right] \sum_{n=0}^{max} P(n)}{t^2} = 0$$

(17)

$$\sigma_D^2 = \sum_{n=0}^{max} \left[\frac{\partial D}{\partial P(n)} \sum_{m=0}^{max} \frac{\partial D}{\partial P(m)} \sigma_{mn} \right] + \sum_{n=0}^{max} \left[\frac{\partial D}{\partial Q(n)} \sum_{m=0}^{max} \frac{\partial D}{\partial Q(m)} \sigma_{mn} \right] \qquad (18)$$

$$\sigma_T^2 = \sum_{n=0}^{max} \left[\frac{\partial T}{\partial P(n)} \sum_{m=0}^{max} \frac{\partial T}{\partial P(m)} \sigma_{mn} \right] + \sum_{n=0}^{max} \left[\frac{\partial T}{\partial Q(n)} \sum_{m=0}^{max} \frac{\partial T}{\partial Q(m)} \sigma_{mn} \right] \qquad (19)$$

A property of the multinomial distribution is that the variance of the total number of multiplicity counts is zero as can be seen. To include a nonzero variance, the singles variance is set to that given by the semi-empircal method which will be explained later:

$$\sigma_S^2 = \frac{\sum_{n=0}^{max} P(n) + \frac{2}{f_d^{theor}} \sum_{n=0}^{max} n(P(n) - Q(n))}{t^2} \qquad (20)$$

An example covariance matrix for the singles, doubles and triples found using this method is given in Table 1.

Once the covariance matrix of the singles, doubles and triples has been attained, the errors for the mass, multiplication and alpha can be found using the same procedure as outlined under the measured error and given by equation 2.

Poisson Distribution

If the total number of counts is taken to be a random variable, as it is in the experiment, then the distribution can also be estimated to be Poisson and every count rate for each multiplicity will be assumed to follow a Poisson distribution. Assuming a Poisson distribution, the process is quite similar to that of the multinomial distribution. The difference lies in the reals plus accidentals distribution P(n) and the accidentals distribution Q(n) covariance matrices. Using a Poisson distribution the matrices are given by:

$$\text{Cov(P(n))}_{ii} = p_i \sum_{n=0}^{max} P(n) = P(i) \qquad (21)$$

$$\text{Cov(P(n))}_{ij} = 0 \qquad (22)$$

where

$$p_i = \frac{P(i)}{\sum_{n=0}^{max} P(n)}$$

and

$$\text{Cov(Q(n))}_{ii} = p_i \sum_{n=0}^{max} Q(n) = Q(i) \qquad (23)$$

$$\text{Cov(Q(n))}_{ij} = 0 \qquad (24)$$

where

$p_i = \frac{Q(i)}{\sum_{n=0}^{max} Q(n)}$ [1]

The covariance matrix for the singles, double and triples is then found just as it was for the multinomial case by equation 16.

$$\text{Cov(SDT)} = X \cdot Cov(P(n)) \cdot X^T + Y \cdot \text{Cov(Q(n))} \cdot Y^T$$

The variance of the singles, doubles and triples is then found to be:

$$\sigma_S^2 = \frac{\sum_{n=0}^{max} P(n)}{t^2} \qquad (25)$$

$$\sigma_D^2 = \frac{\sum_{n=0}^{max} n^2(P(n) + Q(n))}{t^2} \qquad (26)$$

$$\sigma_T^2 = \frac{\sum_{n=0}^{max}\left[\left(\frac{\partial T}{\partial P(n)}\right)^2 P(n)\right] + \sum_{n=0}^{max}\left[\left(\frac{\partial T}{\partial Q(n)}\right)^2 Q(n)\right]}{t^2} =$$

$$\frac{\sum_{n=0}^{max}\left[\left(\frac{n(n-1)}{2} - \frac{\sum_{m=0}^{max} mQ(m)}{\sum_{m=0}^{max} P(m)}\left(n - \frac{\sum_{m=0}^{max} mP(m) - \sum_{m=0}^{max} mQ(m)}{\sum_{m=0}^{max} P(m)}\right)\right)^2 P(n)\right]}{t^2} +$$

$$\frac{\sum_{n=0}^{max}\left[\left(-\frac{n(n-1)}{2} + n\frac{\sum_{m=0}^{max} m(2Q(m) - P(m))}{\sum_{m=0}^{max} P(m)}\right)^2 Q(n)\right]}{t^2} \qquad (27)$$

Another difference between this and the multinomial distribution is that the variance of the singles rate is not zero in this case, and therefore no correction for the singles rate is needed as seen in table 1. However, because multiplicity counting measures time correlated events from fission events, the Poisson distribution is also not an exact estimation as it is valid only for independent processes.

Semi-Empirical

As mentioned above, the rules do not completely apply to use a Poisson or a multinomial distribution and so a semi-empirical technique was created to arrive at the uncertainties for the singles, doubles and triples rates. The procedure to arrive at these equations is quite complex and only a summary is given here. The implementation follows [1] and [3]. The approach taken was to start as if Poisson statistics did apply but to write the Poisson equations in terms of the measured singles, doubles, and triples values and their corresponding accidental rates described below.

The Poisson variance (Eq. 25) can be written in terms of the singles rate (Eq. 7) as:

$$\sigma_S^2 = \frac{\sum_{n=0}^{max} P(n)}{t^2} = \frac{S}{t} \tag{28}$$

and as can be seen, has no corresponding accidental rate.

The doubles rate is harder to see, but if P(n) is thought of as R+A (real plus accidental) distribution and Q(n) is thought of as the A (accidental) distribution, in the calculations for the doubles

$Doubles = \frac{\sum_{n=0}^{max} nP(n) - \sum_{n=0}^{max} nQ(n)}{t}$, the numerator can be thought of as the sum of all the $R+A$ measured neutrons minus the sum of all A measured neutron which gives the rate of total real measured neutrons $D = \frac{R+A-A}{t} = \frac{R}{t}$.

Then when taking the variance of this quantity the Poisson distribution would give $\sigma_D^2 = \frac{R+A+A}{t}$ where R and A are now the real and accidental *rates*. Substituting in D for the reals or R rate we get the Poisson equation in terms of the doubles rate and the doubles accidentals rate.

$$\sigma_D^2 = \frac{D + 2A}{t} \tag{29}$$

A can also be found in terms of the measured singles rate as:

$A = S^2G$ [2]

Where G is the gate length. It can be thought of as $(SG)S$ where SG is the measured neutron count rate times the gate length which would give the expected number of measured neutrons in any random gate times the neutron count rate S which would give you the average expected accidentals rate[2][3].

The triples is treated just like the doubles where the triples rate is thought of as T=$(T + A_T) - A_T$ where A_T is the accidental triples rate. Then, just like the doubles case, the variance of the triples rate is given as:

$$\sigma_T^2 = \frac{T + 2A_T}{t} \tag{30}$$

where

$$A_T = \left(1 + \frac{\gamma}{f_d}\right) S(DG) + \frac{1}{2} S(SG)^2 \tag{31}$$

A_T calculates the accidental triples-coincidences. A triple coincidence event occurs when two triggers occur in the opened gate interval taking into account the combinatorial nature of the scoring. The accidental triples can be split into two categories represented by eq. 31. If the trigger rate captures a double coincidence or if the trigger rate captures a chance pair that happens to be present in the gate. The first case corresponds to the first term in eq. 31 where DG is the expected number of double events per gate and S is the rate at which gates are opened. The multiplier $(1 + \frac{\gamma}{f_d})$ comes about because some of the doubles are associated, while a proportion would be present independent of any temporal association with the triggering event. The second term is simply the random or chance pile-up of uncorrelated events. [3]

f_d represents the fraction of doubles events on the pulse train that fall into the finite reals plus accidentals gate and γ represents the proportion of time correlated doubles events that are actually detected in the accidentals gates. These can be found theoretically if the Dewey profile is represented by a pure exponential with an effective $1/e$ die-away time of τ (which is a good approximation) by:

$$\gamma = 1 - \left(\frac{1 - \exp\left(\frac{-G}{\tau}\right)}{\frac{G}{\tau}}\right)$$

$$f_d = \exp\left(\frac{-P}{\tau}\right)\left(1 - \exp\left(\frac{-G}{\tau}\right)\right)$$

Where τ is the detector die-away time and P is the pre-delay. [4]

After finding these modified Poisson equations a rate specific compensation factor is added to expand the uncertainty to allow for correlations. This compensation factor was found to capture the main functional dependence evident in theory and seen in experiment. Therefore our equations are the modified Poisson equations (28-30) with an added compensation factor δ.

$$\sigma_S^2 = \delta_S \frac{\sum P(n)}{t^2} = \delta_S \frac{S}{t} \tag{32}$$

$$\sigma_D^2 = \delta_D \frac{D + 2A}{t} \tag{33}$$

$$\sigma_T^2 = \delta_T \frac{T + 2A_T}{t} \tag{34}$$

The compensation factors that best agreed with measured data were found as:

$$\delta_S = 1 + \frac{2D}{f_d S}$$

$$\delta_D = 1 + \frac{8\gamma D}{f_d S}$$

$$\delta_T = 1 + \frac{n\gamma D}{f_d S}$$

where n is a factor determined experimentally so that the result would match the measured uncertainty with a typical value of n=10. [1, 3]

Combining these with equations 32-34 the variances are:

$$\sigma_S^2 = \frac{\left(1 + \frac{2D}{f_d S}\right) S}{t} \tag{35}$$

$$\sigma_D^2 = \frac{\left(1 + \frac{8\gamma D}{f_d S}\right)\left(D + 2S^2 G\right)}{t} \tag{36}$$

$$\sigma_T^2 = \frac{\left(1 + \frac{n\gamma D}{f_d S}\right)\left(T + 2A_T\right)}{t} \tag{37}$$

These values can be put into a covariance matrix with the off-diagonals set to zero as seen in Table 1. This matrix can then be used to calculate the uncertainties for the mass, multiplication and alpha using equation 2.

Results and Discussion

An example singles, doubles, and triples covariance matrix for the Poisson, multinomial, and semi-empirical methods are compared with measurement in Table 1.

The relative standard deviation (r.s.d.) of the three methods as well as the measured value are compared in figures 1-18. It can be seen that the multinomial distribution is slightly below the Poisson distribution for all but the corrected singles. The semi-empirical method tends to give the largest r.s.d of the three methods, with the exception of the triples rate, and the closest to the measured value.

The slightly lower variance for the multinomial distribution when compared to the Poisson can be understood when looking at the signs of the derivatives and the covariance matrix. For the doubles variance the terms for the derivatives are always positive as are the variances of the distribution so the product of these terms creates the positive contribution, however, the terms for the co-variances of the distribution always have a negative contribution. Because the variance of the multinomial distribution is smaller than that of the Poisson distribution the doubles error estimations for the multinomial distribution should be smaller than those of the Poisson distribution. The same is true for the triples error except that some covariance terms may have a slightly positive

Measured			Multinomial			Poisson			Semi-Empirical		
7.52	1.69	0.91	4.61*	0	0	2.70	1.05	0.28	4.61	0	0
1.69	1.90	2.22	0	1.96	1.00	1.05	2.45	1.13	0	3.40	0
0.91	2.22	3.45	0	1.00	1.31	0.28	1.13	1.34	0	0	1.47

Table 1: An example singles, doubles, triples covariance matrix calculated from the same measurement of 19.9 g PuO_2. The asterix denotes the value obtained from the semi-empirical approach as suggested by [1].

contribution. However, it is still expected that generally the multinomial triples error estimation will be smaller than that of Poisson.
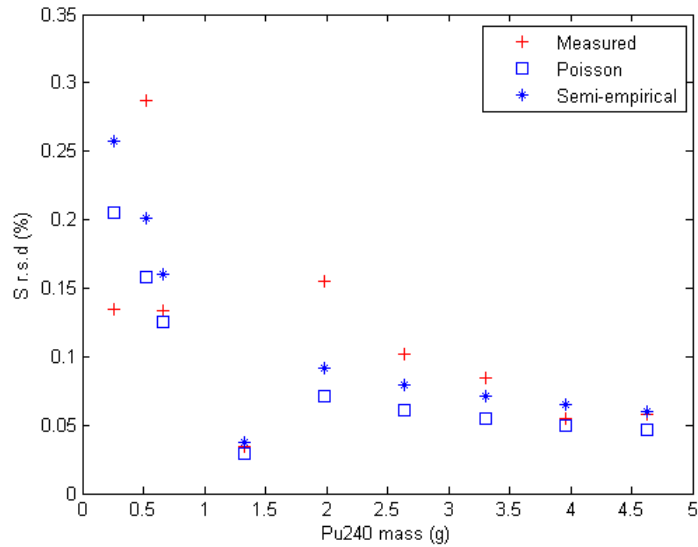
Figure 1: Relative standard deviation of the singles for PuO2: comparison between Poisson, semi-empirical method and measurement.
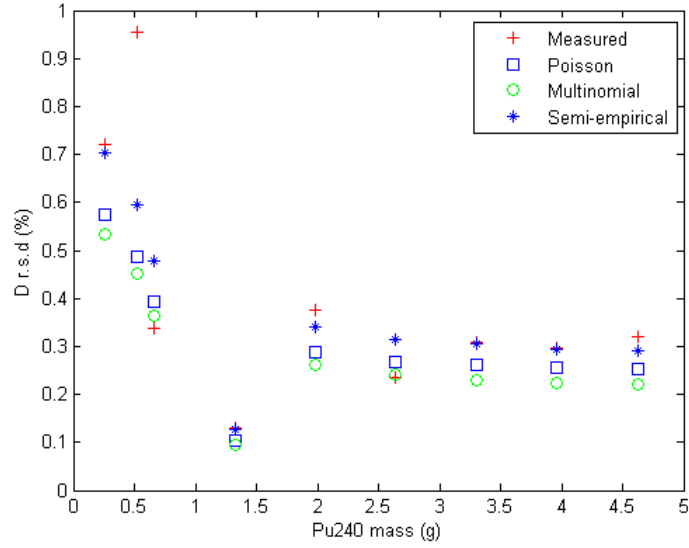
Figure 2: Relative standard deviation of the doubles for PuO2: comparison between Poisson, multinomial and semi-empirical with measurement.
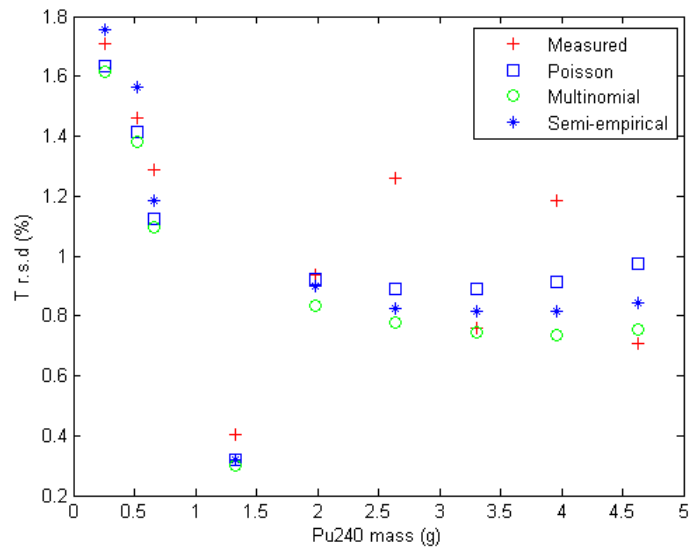
Figure 3: Relative standard deviation of the triples for PuO2: comparison between Poisson, multinomial and semi-empirical with measurement.

11
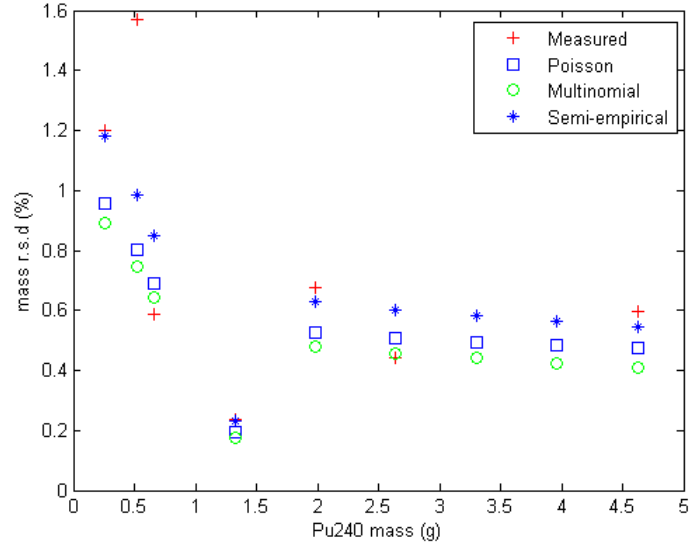
Figure 4: Relative standard deviation of the mass for PuO2: comparison between Poisson and multinomial distributions with measurement.
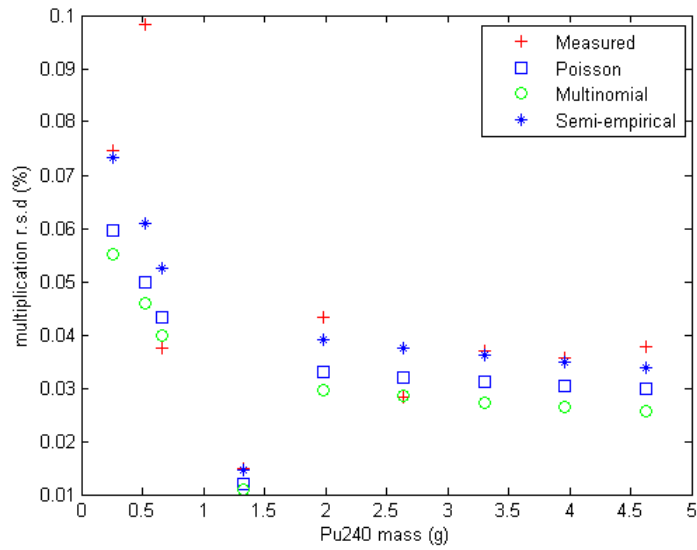
Figure 5: Relative standard deviation of the multiplication for PuO2: comparison between Poisson and multinomial distributions with measurement.

12
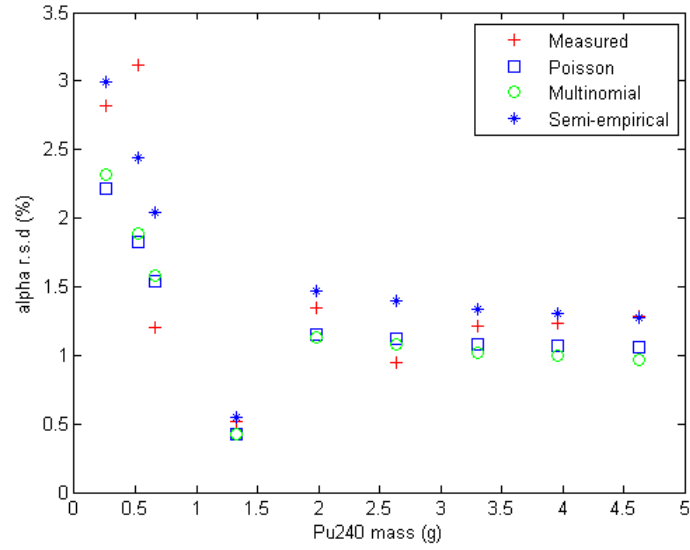
Figure 6: Relative standard deviation of the alpha rate for PuO2: comparison between Poisson and multinomial distributions with measurement.
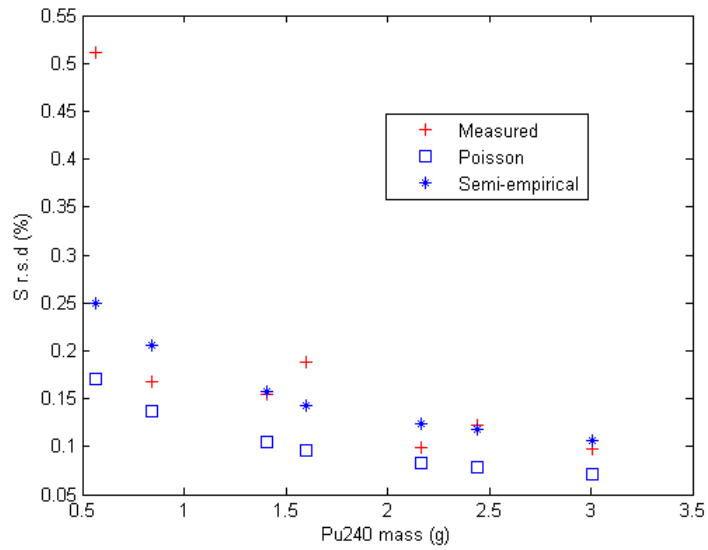
Figure 7: Relative standard deviation of the singles for PM metal: comparison between Poisson, semi-empirical method and measurement.

13
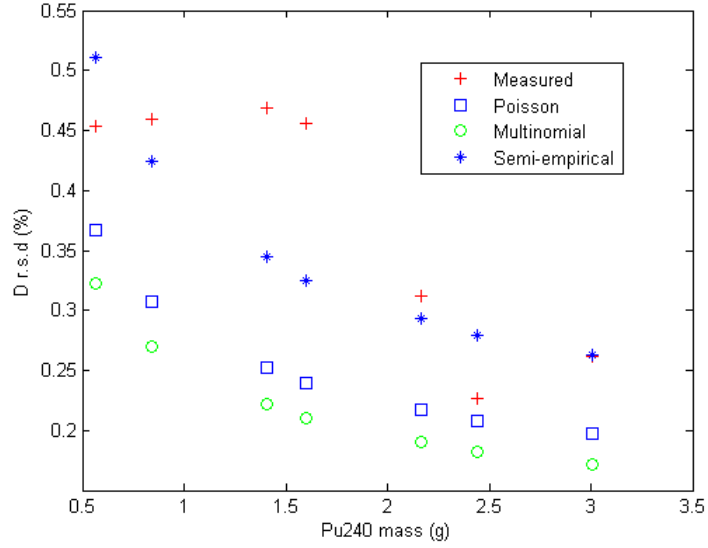
Figure 8: Relative standard deviation of the doubles for PM metal: comparison between Poisson, multinomial and semi-empirical with measurement.
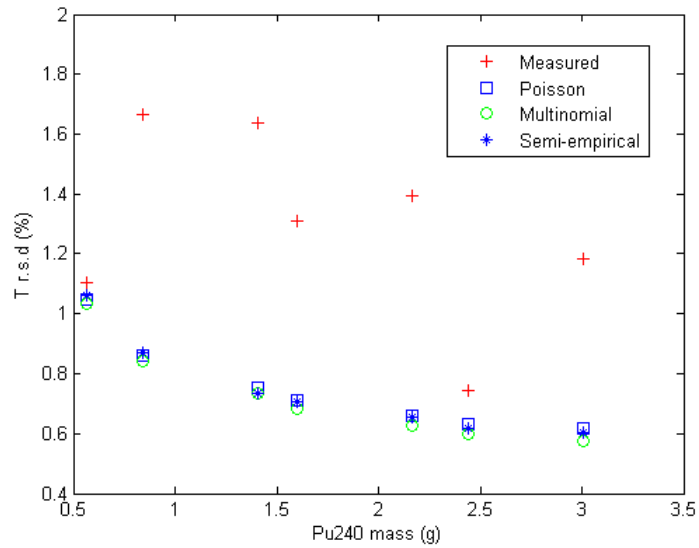
Figure 9: Relative standard deviation of the triples for PM metal: comparison between Poisson, multinomial and semi-empirical with measurement.

14
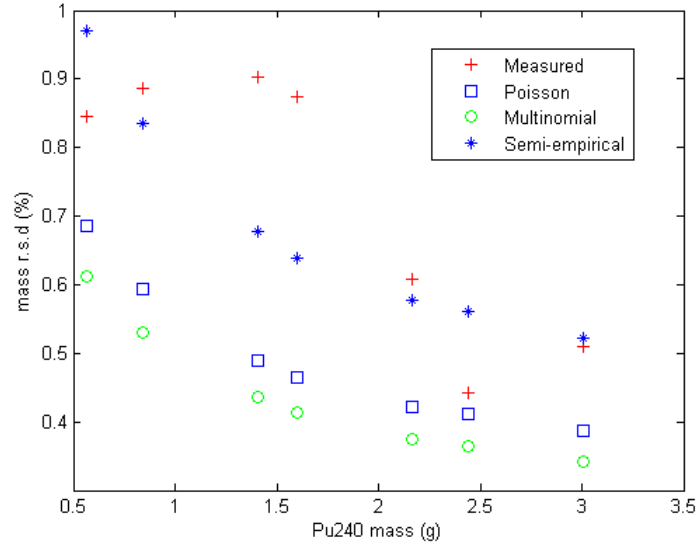
Figure 10: Relative standard deviation of the mass for PM metal: comparison between Poisson and multinomial distributions with measurement.
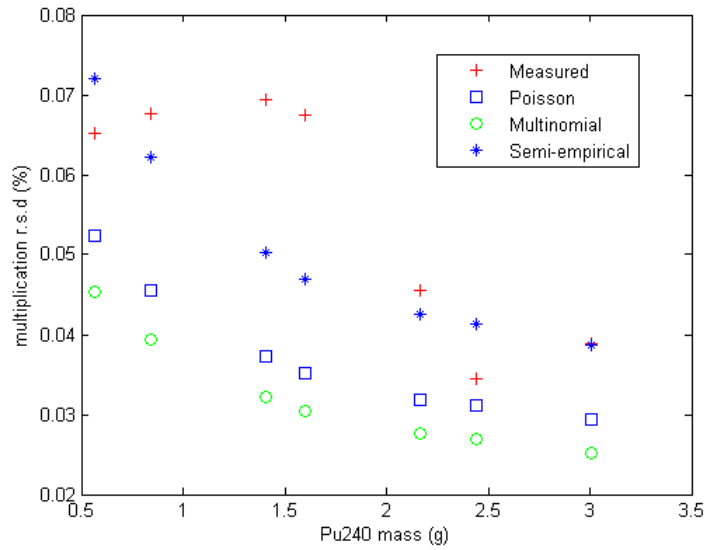
Figure 11: Relative standard deviation of the multiplication for PM metal: comparison between Poisson and multinomial distributions with measurement.

15
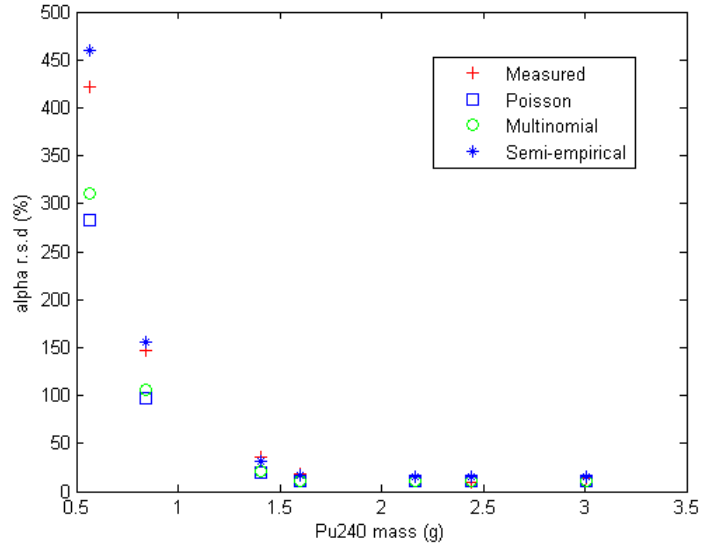
Figure 12: Relative standard deviation of the alpha rate for PM metal: comparison between Poisson and multinomial distributions with measurement.
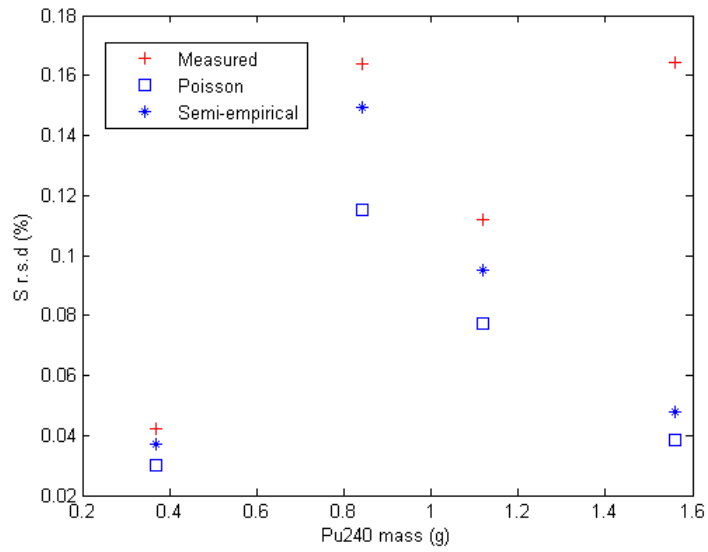
Figure 13: Relative standard deviation of the singles for CBNM: comparison between Poisson, semi-empirical method and measurement.
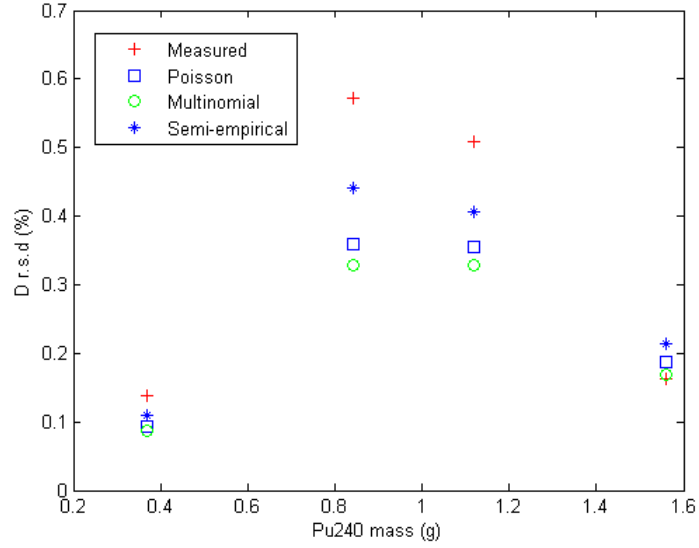
Figure 14: Relative standard deviation of the doubles for CBNM: comparison between Poisson, multinomial and semi-empirical with measurement.
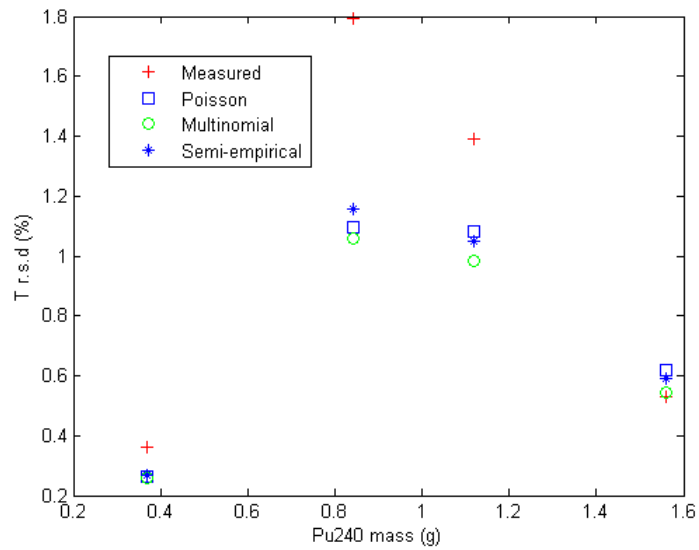
Figure 15: Relative standard deviation of the triples for CBNM: comparison between Poisson, multinomial and semi-empirical with measurement.

17
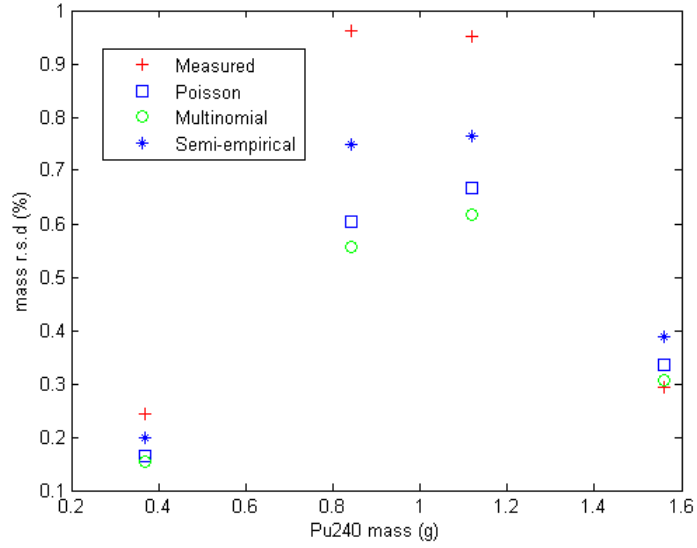
Figure 16: Relative standard deviation of the mass for CBNM: comparison between Poisson and multinomial distributions with measurement.
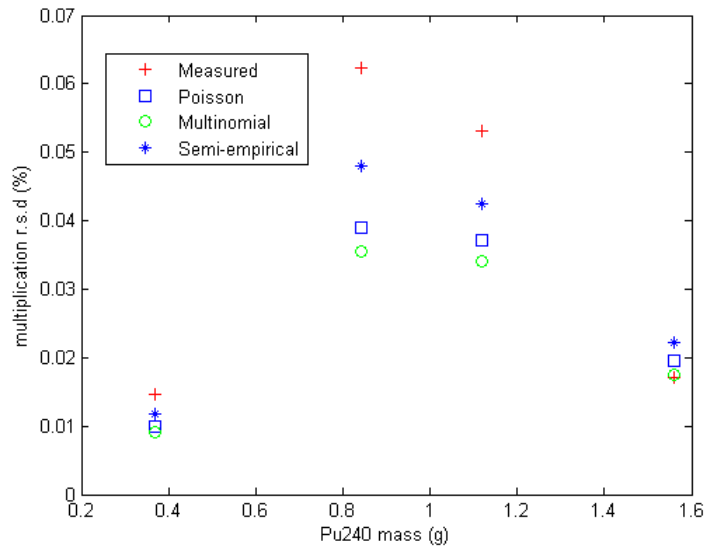
Figure 17: Relative standard deviation of the multiplication for CBNM: comparison between Poisson and multinomial distributions with measurement.

18
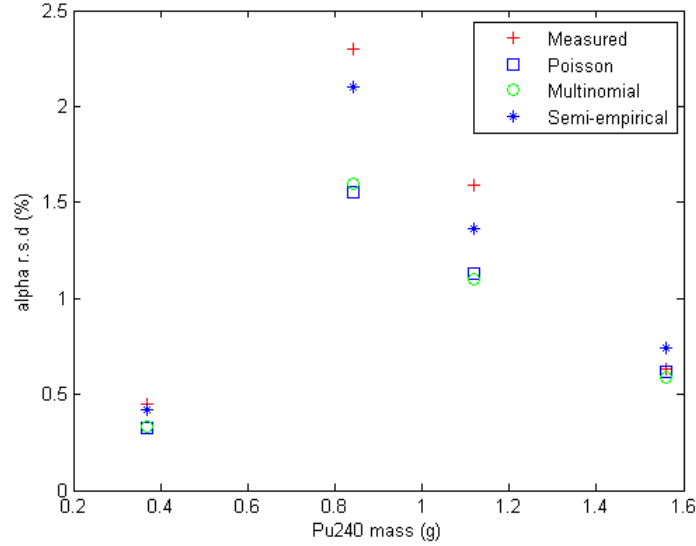
Figure 18: Relative standard deviation of the alpha rate for CBNM: comparison between Poisson and multinomial distributions with measurement.

References

[1] Dytlewski N., Krick M.S. and Ensslin N., Measurement variances in thermal neutron coincidence counting, Nucl. Instrum. & Meths. in Phys. Res., 1991, A327(1193)469-479.

[2] S Croft, LG Evans and M Schear, Optimal gate-width setting for passive neutron multiplicity counting, 51st Annual Meeting of the INMM, July 11-15, 2010, Baltimore, MD, USA.

[3] S Croft, MT Swinhoe, V Henzl, A priori estimation for neuron triples counting, Safeguards Sci. & Technol. Group (N-l), Los Alamos Nat. Lab., Los Alamos, NM, USA.

[4] S Croft, M Schear and LG Evans, Analytical expressions for the gate utilization factors of passive multiplicity counters including signal build-up, 51st Annual Meeting of INMM July 11-15, 2010, Baltimore, MD, USA.